4-30-1981

# Landsat analysis of the dynamics of the Chesapeake Bay plume on the continental shelf

John C. Munday
*Virginia Institute of Marine Science*

Michael S. Fedosh
*Virginia Institute of Marine Science*

# LANDSAT ANALYSIS OF THE DYNAMICS OF THE CHESAPEAKE BAY PLUME ON THE CONTINENTAL SHELF

John C. Munday Jr. and Michael S. Fedosh
Remote Sensing Center
Virginia Institute of Marine Science
School of Marine Science
College of William and Mary
Gloucester Point, Virginia 23062
804/642-2111

Final Report
Contract NA-80-FA-C-00051

National Marine Fisheries Service
Northeast Fisheries Center
Sandy Hook Laboratory
Highlands, New Jersey 07732

April 30, 1981

# LANDSAT ANALYSIS OF THE DYNAMICS OF THE CHESAPEAKE BAY PLUME ON THE CONTINENTAL SHELF

John C. Munday Jr. and Michael S. Fedosh
Remote Sensing Center
Virginia Institute of Marine Science
School of Marine Science
College of William and Mary
Gloucester Point, Virginia 23062
804/642-2111

Final Report
Contract NA-80-FA-C-00051

National Marine Fisheries Service
Northeast Fisheries Center
Sandy Hook Laboratory
Highlands, New Jersey 07732

April 30, 1981

ACKNOWLEDGMENT

For support of this research, we acknowledge and thank the Northeast Fisheries Center, National Marine Fisheries Service, National Oceanic and Atmospheric Administration (Contract NA-80-FA-C-00051), U.S. Department of Commerce. We thank L. Marshall for secretarial assistance.

ABSTRACT

The dynamics of the Chesapeake Bay plume have been studied by examination of 81 dates of Landsat images with color additive enhancement and single-band density slicing. The "plume" was interpreted from surface turbidity discontinuties as revealed in images from multispectral scanner (MSS) bands 4-7. Results show that the Chesapeake Bay plume usually frequents the Virginia coast south of the Bay mouth. Wind and tide vectors are the principal variables affecting the plume dynamics. Southwestern (compared to northern) winds spread and disperse the plume easterly over a large area. Ebb tide images (compared to flood tide images) show a more dispersed plume. Flooding waters produce high turbidity levels over the shallow northern portion of the Bay mouth.

CONTENTS

FIGURES

TABLES

## 1. ADMINISTRATIVE INFORMATION

1.1 Principal Investigator's name: John C. Munday Jr.

1.2 Organization receiving funding: Virginia Institute of Marine Science, College of William and Mary.

1.3 Present (FY 80) funding level: $5,038. Starting date: September 15, 1980.

1.4 Title of work unit or investigation: Landsat Analysis of the Dynamics of the Chesapeake Bay Plume on the Continental Shelf.

1.5 Major NEMP cruises participated in: None.

1.6 Reports or publications produced under this funding:

1) Munday, J.C., Jr. and M.S. Fedosh. 1980. Southern Chesapeake Bay circulation and suspended sediment transport analyzed using Landsat imagery. ACSM-ASP Fall Techn. Mtg., ASP, Falls Church, VA, RS-3-F:1-5.

2) Munday, J.C., Jr. and Michael S. Fedosh. 1981. Chesapeake Bay plume dynamics from Landsat. NASA Conference Publication (Superflux 1980, Williamsburg, VA), in press, 14 p.

1.7 NEMP work unit monitor: James P. Thomas, Chief, Biological Oceanography Investigation.

1.8 Duration that work unit has covered: September 15, 1980 to April 30, 1981.

## 2. OBJECTIVES

The objectives of this research were to use Landsat images to:

1. find the directional pattern of the movement of the out-welling Chesapeake Bay plume,

2. determine the effects of meteorological and physical influences on the direction and rate of plume dispersal,

3. find the seaward extent of the Bay plume, and

4. examine the influence of Eastern Shore inlet plumes on longshore transport of turbidity which is advected into the Bay on flood tide.

## 3. ACTIVITIES AND RATIONALE

### Introduction

A central research question for the Atlantic marine fishery is the distribution of nutrients and pollutants outwelled from coastal bays and estuaries. Investigating the seaward flux of materials, both spatially and temporally, should be fruitful toward understanding fishery productivity and its fluctuations. The plume of the Chesapeake Bay, queen of the east coast estuaries, is attractive to study in this regard from several viewpoints (plume composition, volume discharge, Bay productivity, and Bay-shelf ecology), and has become the initial focus for flux studies coordinated by the NOAA National Marine Fisheries Service.

A leading phase of such study is to resolve the dynamics of the Chesapeake Bay plume. To do so by ship-based study alone would involve prohibitively large effort over long times, therefore, it is advantageous to use remote sensing technology provided by NASA to reduce the effort and provide repetitive synoptic views over large areas. The most striking view is provided by the NASA Landsat satellite, which since its first launch in 1972 has produced over eighty cloud-free images of the lower Chesapeake Bay region. The limitations of Landsat for Bay plume study are recognized -- the sensors primarily discriminate suspended sediment in the upper few metres of the water column, and the images are only snapshots of continuous dynamic processes -- nevertheless, Landsat can provide an overview of the plume dynamics which is useful in guiding future aerial remote sensing and ship-based investigations.

In this study a large set of Landsat images has been examined using visual methods and image enhancement devices. The principal objective has been to determine what continental shelf regions are frequented by the Bay plume. A second objective has been to determine the effects of tidal phase and wind on plume dynamics.

This study was conducted in relation to the NOAA/NMFS-sponsored Superflux program, which investigated the effects of the Chesapeake Bay plume on continental shelf waters. Although cloud-free Landsat passes did not occur during the Superflux cruises, the activities under this contract were closely tied to the objectives of the Superflux program. This was made possible through active participation by the Principal Investigator in all Superflux planning and review meetings.

### Methods

Eighty-one dates of cloud-free Landsat images of the southern Chesapeake Bay (path 15, row 34) were obtained from the USGS EROS Data Center, Sioux Falls, South Dakota. The overpass times cover the phases of the

diurnal tidal cycle at 10 to 20 minute intervals (Figure 1a). The dates cover all months of the year at shorter than 15 day intervals (Figure 1b). Sixty-five of the images are in the format of 18.5 cm (1:1,000,000) positive transparencies of MSS band 5; for 48 dates of the total, the images are 70 mm (1:3,369,000) positive transparencies of MSS bands 4, 5, 6, and 7. Dates and formats of the imagery are given in Table 3, Data Inventory. With images already on hand, the total is 94 dates.

Wind data were obtained from the Norfolk Regional Airport weather station covering the twelve hours preceding each overpass at 3-hour intervals. These data were vector-averaged for each pass; the composite wind regime for all passes is shown in Figure 2a, compared to the 1946-1970 record for Norfolk in Figure 2b. For use in image analysis the wind data of Figure 2a were grouped into the quadrants 0-89° (+0, 90, 180, and 270°) labeled 1, 2, 3, and 4.

The methods of image analysis included visual interpretation coupled with machine-assisted enhancement. Two interpreters analyzed each 18.5 cm image on a light table; the first interpreter traced turbidity boundaries manually based on visual inspection, and the second checked the tracing, making modifications as needed. The 70 mm images were enhanced with an International Imaging Systems ($I^2S$) color additive viewer, and the color enhancements were photographed on color slide (35 mm) film for projection during later analysis. Each 18.5 cm image was enhanced with an $I^2S$ 32-channel optical density analyzer with a vidicon, digital processor, and color-coded television display. A black mask covering land areas was used during this analysis to focus attention on water patterns; that the mask had negligible effect on the density analysis was evidenced by the constancy of patterns when the image was rotated through 90° (the danger is that electronic band width limitations during scanning across sharp brightness gradients will cause smearing in the color-coded output). The display was photographed on color slide (35 mm) film for projection during later analysis. Also, a contour map of optical density was prepared from the display by placing an acetate sheet on the $I^2S$ light table and manually drawing contours while viewing the display monitor; this procedure produced contour maps at the original image scale.

The above procedures produced two types of maps. The one consists of visually-discriminated turbidity boundaries extending sometimes over long distances, possibly through background turbidity gradients not noticeable visually. These background gradients would be weak, because the eye during the mapping process ignores weak gradients, but enhances sharp gradients and emphasizes the continuity of turbidity-marked hydrodynamic features over long distances. The second type of map is of photographic density contours which qualitatively picture the absolute turbidity levels. With appropriate calibration this type of map could become a map of absolute concentrations of suspended solids.

In the contour map, a plume with a turbidity gradient will be dissected by the density contouring and may fail to be noticed. On the other hand, the $I^2S$ is more sensitive than the eye to weak density changes, revealing

turbidity boundaries which would not be detected by visual analysis alone. It is emphasized that visual maps and density contour maps enhance different aspects of an image and should not be expected to be similar. Examples of the maps are shown in Figure 3; negative copies of several 18.5 cm MSS 5 images (with masking of the land areas) are shown in Figure 4, and additional full-size images are in the Appendix.

Patterns on the original 18.5 cm images and on the several data reduction products were simultaneously compared during extraction of measurements. Measurements were based on a 1 mm grid overlay (graph paper) facilitating use of the image scale of 1 mm:1 km. The distance and direction of plume-related features were measured with respect to an origin at 37° N latitude/76° W longitude. Azimuthal sectors and 1 cm grid squares frequented by turbid boundaries associated with the plume were determined using the sector and grid map in Figure 5: when an edge of the "plume" was noticed at some radial distance and direction from the origin, sector/zone segments radially outward to this position were "counted" (as having been "visited"). Simple relationships were then sought between the spatial distribution of counts and several variables including wind direction by quadrants (from 12-hour average wind vectors), wind speeds, wind duration, tidal phase, bathymetry, passage of weather fronts, and fresh water inflow into the Bay.

For this project, it has been possible to complete only some spatial analysis and statistical analysis using single-variable statistics. Further work is needed using multi-variate methods.

## 4. DEFINITION OF THE "PLUME"

The counting of areas as "visited" was based only on the presence of turbidity discontinuities which appeared to be significant with respect to Chesapeake Bay plume dynamics. This counting policy was made deliberately wide and somewhat vague, because of the lack of historical data on plume dynamics. It gave the interpreters much freedom of choice. In subsequent studies, a more restrictive policy can be used based on the results obtained here.

There are several consequences of the above policy. First, some of the features of turbidity which were "counted" may be associated, not with the plume, but with along-shore currents. According to Bumpus (1973), there is generally a net non-tidal southerly current along the Eastern Shore and Virginia-North Carolina borders toward Cape Hatteras. This current could involve shear and turbidity gradients (some images give the impression of turbidity discontinuities parallel to shore at the 30 m isobath). Second, studies by Harrison et al. (1967), Johnson (1976), and Ruzecki et al. (1976) show that flow adjacent to Cape Henry is rotary, that the general southerly flow is sporadic rather than continuous, and that flow is wind-influenced in the along-shore direction. These findings should be considered in the interpretation of any observed features.

Third, it is probable that the collection of plume features on any one image is derived from several tidal cycles. In this regard, the distance of features from the mouth should be helpful in discriminating the different cycles. Drogue data published by Johnson (1976) and Ruzecki et al. (1976) suggest that the tidal excursion at the Bay mouth is only about 8 km, whereas at the Chesapeake Light Station (23 km east) the tidal excursion is negligible. Thus, features beyond 15-20 km almost certainly result from non-tidal flow and the net movement from several cycles of tidal flow.

However, apart from the distance factor, the features themselves do not suggest a distinction between features for the cycle in progress from those for preceding cycles. Distinguishing sequential plumes using multispectral satellite images was first described by Mairs and Clark (1973); their approach was not successful here because plumes are too faint on the small set of multispectral images on hand. Defining plumes more clearly using digital processing of Landsat CCT data should prove useful. In contrast, for the smaller plumes from the Eastern Shore inlets, the distinction of sequential tidal cycles is possible on single band images; the inlet plumes often have the appearance of a sequence of turbidity pulses.

Fourth, it should be noted that Landsat records upwelling radiance from only the surface layers. The depth of the observed turbidity varies inversely with its opacity, with the depth of observation for prevailing

turbidities being perhaps 5 m. Thus, plume features at greater depth are not recorded. Also, higher turbidities are produced by scour and resuspension over shallow depths, with the consequence that turbidity levels become decoupled from plume waters per se. Generally, then, Landsat is not always recording plume water boundaries as defined by vertical profiles of temperature, salinity, nutrients and biological variables.

## 5. RESULTS AND INTERPRETATION

More than half of the Landsat images revealed clear evidence of a Bay plume using the different analysis methods. Most of the remaining images showed some evidence of a plume, but not as clearly. It must be noted that the small residue of cloud-free images lacking distinct plume evidence nevertheless provide clues for plume occurrences.

### Eastern Shore

The imagery suggests no dominant direction of longshore transport along the ocean-side of the Eastern Shore. Some images suggest a gyre system off Chincoteague Inlet. Suspended sediment from the southerly inlets is seen in flood tide images to be connected with turbid plumes on the north side of the Bay mouth.

It is well-known that patterns of turbidity are strongly and immediately influenced by changes in wind direction and speed (Doebler, 1966). On the ocean-side of the Eastern Shore, turbid water is associated with areas less than 10 m deep, the degree of turbidity depending on wind direction. Shallow areas off Ocean City, Maryland are usually wind-influenced, judging from the downwind-trending plumes.

### Bay Mouth

Ebb tide plumes can be seen off the south side of the Bay mouth. Turbidity patterns suggest that flood tide is stronger on the north side of the mouth, while ebb is stronger on the south, perhaps influenced by the Coriolis force (Ludwick and Melchor, 1972; Munday and Fedosh, 1980). The imagery suggests that the suspended sediment for the ebb plumes originates in the western portion of the Bay below the Rappahannock River, and especially from the James River jet (Ludwick, 1973). Bay mouth waters appear generally turbid in winter and spring, while in summer and fall, turbid water is more associated with areas less than 10 m deep.

The Bay mouth waters are turbid (except over deeper channels) during winter and spring. During these seasons the winds are mainly northerly with higher than average wind speeds. The Bay axis, parallel to these winds, provides a longer fetch allowing for larger waves which can mix the water column and stir up bottom sediment. The deeper water is not disturbed, thus the reduced turbidity over channels. Doebler (1966) also found higher tides at the Bay mouth with northerly winds.

In the summer and fall the Bay mouth waters appear less turbid. During these seasons the winds are southerly and westerly at lower speeds. Winds from these directions apparently do not have a large enough fetch to create waves of sufficient height and strength to stir up bottom

sediments. The seasonal variation of wind speed was noted by Ludwick and Melchor (1972) who found that, during the winter, 45 days had winds greater than 15 mph, compared to 10 days in summer.

The ebb plumes exiting the southern portion of the Bay mouth have their directional movement influenced by wind, the plume trending downwind. The direction of plume movement ranges from east to south. Eastward trending plumes extend approximately 40 km beyond the Bay mouth; southward trending plumes, not influenced by wind, are within 15 km of shore.

There appears to be no Ekman transport effect, because plumes usually are oriented downwind. Doebler (1966) did find a surface drift angle range of 4.8° to 13.2° to the right. He found that summer and offshore currents were further to the right of wind. This was due to a decrease of dynamic viscosity in strongly stratified summer waters causing less downward transfer of momentum. Moderate winds had drift currents to the right of strong winds presumably because, in shallow waters, strong winds mix the water vertically and cause driven currents to "feel" the bottom.

The Norfolk wind data for the Landsat images are similar to the average Norfolk winds (Figure 2). There is little correlation between wind data from Patuxent, Maryland, and Norfolk wind data: the correlation coefficient is 0.1465. The predominant wind directions at both stations appear influenced by open water: for Patuxent, to the northwest; and for Norfolk, to the north and northeast.

The ebb plume suspended sediment originates mainly from the James River (Ludwick, 1973) and the western portion of the Bay below the Rappahannock River. Some images show high discharge related plumes entering the Bay from the Potomac River. It is not known whether this suspended sediment reaches the Bay mouth; however, high fresh water flow at Washington, D.C. lowers salinity off the Bay mouth two months later (Howe, 1952), which suggests a very long persistence to different water masses despite tidal action. For the James River, Hurricane Camille water required three days to reach Hampton Roads from Richmond (Elder, 1971). Slightly above-average fresh water flow at Richmond takes about six days to affect water heights at Hampton Roads.

## Composites of Observed Boundaries

Composites of the turbid boundaries seen on all the images divided into flood and ebb tide groups are shown in Figure 6. Viewed in the manner of a geologic fault map, the ebb tide composite shows most "lineaments" found between Cape Charles and Cape Henry are oriented toward 120°. The flood tide lineaments although more random are oriented similarly. In both cases, most lineaments beyond the mouth are found near the coast southward; only a few lineaments beyound the mouth are found toward 40° to 90°. An initial hypothesis was therefore that the plume usually frequents the southeasterly direction. Subsequent analysis was oriented toward testing this hypothesis.

Sector/Zone Count Analyses

The map in Figure 7a shows sector/zone counts for all wind classes and tidal phases; zones A through E for sectors at $\theta \sim 150^{o}$ are the most frequently visited. Sorting the pass dates by wind quadrant, $Q_i$, yields $Q_1$ = 20 images, $Q_2$ = 3, $Q_3$ = 41, $Q_4$ = 17. Maps for the wind quadrants are shown in Figures 7b-d (a map is omitted for $Q_2$ because of its low value). $Q_4$ produced the tightest pattern along the Virginia-North Carolina coast; $Q_3$ (southwest winds) produced the most dispersed pattern (notice especially the visits to zones D-F for $\theta \sim 90^{o}$).

To enhance the differences between results from different wind quadrants, ratios have been formed of sector/zone counts using the quadrants 3 over 1, and 4 over 1. Counts for each quadrant were adjusted upward by 1 count for each pass where no plume was discriminated (which in effect produces a contrast stretching of the ratios): the adjustment frequencies for each quadrant were 1, 1, 6, and 0 respectively. The ratios were then normalized for differences among the $Q_i$ values. The resulting ratios R are shown in Tables 1 and 2. Numerical values of R near 1.0 indicate no difference in effects of wind direction for the two quadrants under consideration. Table 1 (quadrants 3 over 1) shows $R > 1$ for $\theta < 140^{o}$ (zones B-E), a clear demonstration that southwest (compared to northeast) winds disperse the plume over a larger area and swing its dominant direction away from the southeast toward the east. Table 2 (quadrants 4 over 1) demonstrates that northwest (compared to northeast) winds constrain the plume to the coastline toward the southeast.

TABLE 1

NORMALIZED RATIOS OF COUNTS

FOR WIND QUADRANT 3 OVER QUADRANT 1

| Zone \ Sector | 6* | 7 | 8 | 9 | 10 | 11 | 12 | 13 | 14 | 15 | 16 |
|---|---|---|---|---|---|---|---|---|---|---|---|
| A | 1.46 | 1.46 | 1.46 | 1.27 | 0.91 | 0.98 | 1.12 | 0.92 | 0.77 | 0.83 | 0.84 |
| B | ∞ | 2.93 | 1.95 | 2.44 | 1.83 | 1.83 | 1.95 | 1.66 | 1.25 | 0.84 | 0.88 |
| C | 3.41 | 4.39 | 4.88 | 2.68 | 1.79 | 1.34 | 2.11 | 1.71 | 0.98 | 0.80 | 0.98 |
| D | 3.90 | 3.90 | 4.39 | 4.39 | 3.90 | 4.39 | 4.39 | 2.44 | 1.46 | 0.98 | 0.98 |
| E | 2.93 | 3.41 | 3.41 | 3.41 | 3.41 | 3.41 | 3.41 | 2.93 | 1.46 | 1.30 | 1.22 |

* $10^{o}$ interval from $60^{o}$ to $70^{o}$; similarly for all sectors.

TABLE 2

NORMALIZED RATIOS OF COUNTS

FOR WIND QUADRANT 4 OVER QUADRANT 1

| Zone \ Sector | 6* | 7 | 8 | 9 | 10 | 11 | 12 | 13 | 14 | 15 | 16 |
|---|---|---|---|---|---|---|---|---|---|---|---|
| A | 0 | 0 | 0 | 0.24 | 0.17 | 0.34 | 1.01 | 1.18 | 1.01 | 1.09 | 1.02 |
| B | | 0 | 0 | 0.39 | 0.29 | 0.29 | 0 | 1.88 | 1.57 | 1.01 | 1.02 |
| C | | | | 0 | 0 | 0 | 0 | 0.29 | 1.18 | 1.32 | 1.62 |
| D | | | | | | | | 0 | 0.39 | 0.94 | 1.18 |
| E | | | | | | | | | 0 | 0.39 | 0.29 |

* 10° interval from 60° to 70°; similarly for all sectors.

Sector-count maps for flood versus ebb tide in Figure 8 show somewhat more dispersion of plume features for ebb tide. A subset of the ebb tide data for southwest winds ($Q_3$) higher than 8 knots included only five images; in these images a plume could not be discriminated. These results are further evidence that southwest winds disperse the plume on ebb tide.

In subsequent study, polar coordinates were determined for the most distant point on each plume. The results for flood and ebb tides and wind quadrants $Q_1$, $Q_3$, and $Q_4$, are shown in Figure 9a through 9f. The results are similar to the earlier results. The results show that southwestern winds for passes during ebb tide are associated with the greatest dispersion and extension of the plume. For northern winds, plumes for all tidal phases are found close to Virginia Beach.

Cape Charles Grid Analysis

Many images reveal turbidity in late-ebb/early-flood, located adjacent to Fisherman's Island (at the tip of Cape Charles) on the north side of the Bay mouth (Munday and Fedosh, 1980). The patterns suggest that early flood waters moving into the northern side of the Bay mouth carry residual suspended sediment from the Eastern Shore nearshore zone, and additional material resuspended in the shallow areas adjacent to Fisherman's Island. If true, turbidity on the western side of the mouth (compared to the eastern side) should be relatively more frequent during flood, as flooding waters traverse increasing areas of shallows.

To test this hypothesis quantitatively using Landsat images, a counting procedure was employed based on the square grid shown in Figure 5. A cell was counted when turbidity in the cell was higher than background as judged visually. Counts were made for ebb and flood tide passes and subset into the four wind quadrants. Ratios of flood to ebb counts were formed

and normalized for flood and ebb pass frequencies; the normalized ratios truncated to integers are shown in Figure 10a. Western cells are, as expected, relatively more frequented by turbidity than eastern cells during flood tide. Truncated normalized ratios for the wind quadrants are shown in Figure 10b for Q1 over Q3, and Figure 10c for Q1 over Q4 (Figure 10c numbers were multiplied by 2 before plotting). Figures 10b and 10c demonstrate that western (compared to northeastern) winds reduce western and increase eastern turbidities.

Wind Duration and Wind Speed

Correlation and regression analyses have been performed on wind speed and wind duration versus plume extension, with tidal phase and wind quadrant as parameters. None of the analyses have yet produced statistically significant results. Multivariate statistical methods will be utilized for further analysis. Perhaps appropriate measures of the plume have yet to be discovered.

Discussion

Image analysis has shown that the "plume" (as broadly defined here) usually frequents the southeasterly direction (120°-150° relative to the mouth). Passes during ebb (compared to flood) show a somewhat more dispersed plume. Southwestern winds are effective in dispersing and extending the plume, especially on ebb tide passes, while for northern winds plumes remain close to Virginia Beach.

These effects of winds have been shown using vector-averaged Norfolk wind data from the 12 hours preceding the Landsat overpass. Because the shelf water relaxation time from wind effects is probably greater than 12 hours, longer wind records should be studied. Also, Chesapeake Light Tower winds would perhaps be more appropriate than Norfolk winds for examining the effect of shelf water currents on the plume dynamics.

For flood tide, a striking feature of many images is a strong turbidity pattern on the shallow northern side of the Bay mouth adjacent to Fisherman's Island. The pattern suggests a predominance of the northern side during flood tide, due to the Coriolis force and southerly drift along the Eastern Shore. Analysis shows that the turbidity is relatively greater in flood tide and northeastern winds. No such patterns were observed for flood tide in the southern portion of the Bay mouth; in addition to the Coriolis deflection toward the north, the water in the southern portion is much deeper, reducing surface turbidities which originate in tidal scour.

For ebb tide, the plume for northerly winds is tongue-shaped, but the shape is difficult to characterize further. Little was observed which would suggest rotary motion off Cape Henry as observed by Harrison *et al.* (1967).

## 6. DATA INVENTORY

Table 3 shows the inventory of data obtained for the research. All data are on file in the Remote Sensing Center, Virginia Institute of Marine Science, Gloucester Point, Virginia, 23062 (804/642-2111, ext. 254).

The wind data were obtained from the National Climatic Center, Asheville, North Carolina, 28801 (704/258-2850). The tide data were obtained from the National Oceanic Survey, Tidal Data Datum Branch, Code C 233, 6001 L. Executive Boulevard, Rockville, Maryland, 20852 (301/443-8467). The fresh water discharge data were obtained from U.S. Geological Survey reports on yearly river flow in Virginia (Water Resources Data for Virginia: Water Year 1971 to 1979, U.S. Geological Survey Water Data Report VA: 71-79, NTIS, Springfield, VA).

Table 4 shows the wind data for 1000 hours EST, near the overpass times, which varied between 1345 and 1514. Table 4 also shows the average of winds for the Norfolk station for 24-hour and 5-day periods ending at 1000 hours EST on the date of the overpass.

Table 5 shows the tide data for Sewells Point.

TABLE 3

LANDSAT IMAGERY AND ASSOCIATED ENVIRONMENTAL DATA

FOR THE SOUTHERN CHESAPEAKE BAY#

| | | Wind Vector | | | Bands of Images B&W Film Positive | | | |
|---|---|---|---|---|---|---|---|---|
| | Date | Patuxent NAS, MD | Norfolk Airport, VA | Tide Data Sewells Pt. | 70 mm MSS 5 only | 70 mm MSS 4-7 | 18.5 cm MSS 5 only | 18.5 cm MSS 4-7 |
| 94. | 3 Dec 79 | X | X | X | | X | X | |
| 93. | 15 Nov 79 | X | X | X | | X | X | |
| 92. | 28 Oct 79 | X | X | X | | X | X | |
| 91. | 19 Oct 79 | X | X | X | | X | X | |
| 90. | 3 Jul 79 | X | X | X | | X | X | |
| 89. | 1 May 79 | | X | X | | X | X | |
| 88. | 22 Apr 79+ | | X | X | X | | | |
| 87. | 17 Mar 79 | X | X | X | | X | | |
| 86. | 4 Jan 79 | X | X | X | | X | | |
| 85. | 26 Dec 78 | X | X | X | | X | X | |
| 84. | 27 Sep 78+ | | X | | X | | X | |
| 83. | 18 Sep 78 | X | X | | | X | X | |
| 82. | 22 Aug 78 | X | X | | | X | X | |
| 81. | 4 Aug 78 | X | X | X | | | X | |
| 80. | 17 Jul 78 | X | X | X | | | X | |
| 79. | 8 Jul 78 | X | X | X | | | X | |
| 78. | 29 Jun 78 | X | X | X | | | X | |
| 77. | 20 Jun 78 | X | X | X | | | X | |
| 76. | 11 Jun 78 | X | X | X | | | X | |
| 75. | 9 Apr 78 | X | X | X | | | X | |
| 74. | 31 Mar 78+ | | X | | X | | X | |
| 73. | 4 Mar 78 | X | X | | | X | X | |
| 72. | 27 Jan 78 | X | X | | | X | X | |
| 71. | 28 Dec 77+ | | X | | X | | | |
| 70. | 22 Dec 77 | X | X | X | | X | X | |

| | | Wind Vector | | | Bands of Images B&W Film Positive | | | |
|---|---|---|---|---|---|---|---|---|
| | Date | Patuxent NAS, MD | Norfolk Airport, VA | Tide Data Sewells Pt. | 70 mm MSS 5 only | 70 mm MSS 4-7 | 18.5 cm MSS 5 only | 18.5 cm MSS 4-7 |
| 69. | 11 Oct 77 | | X | | | X | X | |
| 68. | 29 Sep 77+ | | X | | X | | X | |
| 67. | 11 Sep 77+ | | X | | X | | X | |
| 66. | 5 Sep 77 | X | X | | | X | X | |
| 65. | 6 Aug 77+ | | X | | X | | X | |
| 64. | 19 Jul 77 | X | X | X | | | X | |
| 63. | 7 Jun 77+ | | X | | X | | X | |
| 62. | 8 May 77 | X | X | X | | X | | |
| 61. | 14 Apr 77 | X | X | X | | X | | |
| 60. | 9 Mar 77 | X | X | X | | | X | |
| 59. | 25 Feb 77 | X | X | X | | | X | |
| 58. | 1 Feb 77 | X | X | | | X | X | |
| 57. | 27 Dec 76 | X | X | | | X | X | |
| 56. | 9 Dec 76 | X | X | | | X | X | |
| 55. | 21 Nov 76 | X | X | X | | X | | |
| 54. | 3 Nov 76+ | | X | | X | | | |
| 53. | 16 Oct 76 | X | X | | | X | X | |
| 52. | 23 Aug 76 | X | X | X | | X | | |
| 51. | 5 Aug 76+ | | X | X | X | | | |
| 50. | 27 Jul 76+ | | X | X | | | | X |
| 49. | 12 Jun 76+ | | X | X | | | | X |
| 48. | 25 May 76+ | | X | X | | | | X |
| 47. | 28 Apr 76 | X | X | X | | | X | |
| 46. | 10 Apr 76 | X | X | X | | X | X | |
| 45. | 1 Apr 76 | X | X | X | | | X | |
| 44. | 23 Mar 76 | X | X | X | | | X | |
| 43. | 5 Mar 76 | X | X | X | | | X | |
| 42. | 25 Feb 76 | X | X | X | | | X | |
| 41. | 7 Feb 76 | X | X | X | | | X | |
| 40. | 20 Jan 76 | X | X | X | | X | X | |
| 39. | 2 Jan 76 | X | X | X | | | X | |
| 38. | 24 Dec 75 | X | X | X | | | X | |
| 37. | 18 Nov 75 | X | X | | | X | X | |

| | | Wind Vector | | | Bands of Images B&W Film Positive | | | |
|---|---|---|---|---|---|---|---|---|
| | Date | Patuxent NAS, MD | Norfolk Airport, VA | Tide Data Sewells Pt. | 70 mm MSS 5 only | 70 mm MSS 4-7 | 18.5 cm MSS 5 only | 18.5 cm MSS 4-7 |
| 36. | 31 Oct 75 | X | X | X | | | X | |
| 35. | 22 Oct 75 | X | X | X | X | X | X | |
| 34. | 13 Oct 75 | X | X | X | X | X | X | |
| 33. | 4 Oct 75 | X | X | X | | | X | |
| 32. | 29 Aug 75 | X | X | X | | | X | |
| 31. | 20 Aug 75 | X | X | X | | | X | |
| 30. | 11 Aug 75+ | | X | X | | | | X |
| 29. | 2 Aug 75 | X | X | X | | | X | |
| 28. | 18 Jun 75 | X | X | X | | | X | |
| 27. | 9 Jun 75 | X | X | X | | | | X |
| 26. | 22 May 75+ | | X | X | | | | X |
| 25. | 13 May 75+ | | X | X | | | | X |
| 24. | 25 Apr 75+ | | X | | X | | | |
| 23. | 21 Feb 75 | X | X | X | | | X | |
| 22. | 11 Dec 74+ | | X | | X | | | X |
| 21. | 23 Nov 74 | X | X | X | | | X | |
| 20. | 18 Oct 74+ | X | X | X | X | | | X |
| 19. | 12 Sep 74 | X | X | X | | | X | |
| 18. | 20 Jul 74 | X | X | X | | | X | |
| 17. | 21 Apr 74 | X | X | X | | | X | |
| 16. | 3 Apr 74 | X | X | X | | X | X | |
| 15. | 26 Feb 74 | X | X | X | | | X | |
| 14. | 28 Nov 73+ | | X | X | | | | X |
| 13. | 10 Nov 73+ | | X | X | | | | X |
| 12. | 23 Oct 73 | X | X | | | | | X |
| 11. | 5 Oct 73+ | | X | X | | | | X |
| 10. | 17 Sep 73+ | | X | X | | | | X |
| 9. | 30 Aug 73+ | | X | | X | | X | |
| 8. | 12 Aug 73 | X | X | X | | | X | |
| 7. | 25 Jul 73+ | | X | X | | | | X |
| 6. | 1 Jun 73 | X | X | X | | | | X |
| 5. | 14 May 73+ | | X | X | | | | X |
| 4. | 13 Feb 73 | X | X | X | | | X | |

| | | Wind Vector | | | Bands of Images B&W Film Positive | | | |
|---|---|---|---|---|---|---|---|---|
| | Date | Patuxent NAS, MD | Norfolk Airport, VA | Tide Data Sewells Pt. | 70 mm MSS 5 only | 70 mm MSS 4-7 | 18.5 cm MSS 5 only | 18.5 cm MSS 4-7 |
| 3. | 26 Jan 73 | X | X | X | | X | X | |
| 2. | 3 Dec 72 | X | X | X | | | | X |
| 1. | 10 Oct 72 | X | X | | | X | X | |

# Date of Preparation: April 30, 1981.

+ Clouds over significant portion of image.

TABLE 4

WIND DATA

| | Date | 1000 Hours EST Norfolk Dir. (°) | Norfolk Speed (knots) | Patuxent Dir. (°) | Patuxent Speed (knots) | Wachapreague Dir. (°) | Wachapreague Speed (knots) | 24-Hour Norfolk Dir. (°) | 24-Hour Norfolk Speed (knots) | 5-Day Norfolk Dir. (°) | 5-Day Norfolk Speed (knots) |
|---|---|---|---|---|---|---|---|---|---|---|---|
| 94. | 3 Dec 79 | 10 | 13 | 0 | 8 | 340 | 6 | 344 | 8.8 | 301 | 5.5 |
| 93. | 15 Nov 79 | 330 | 6 | 300 | 6 | 270 | 3 | 353 | 8.1 | 21 | 13.8 |
| 92. | 28 Oct 79 | 250 | 10 | 210 | 10 | 200 | 18 | 222 | 6.8 | 359 | 3.4 |
| 91. | 19 Oct 79 | 80 | 5 | 140 | 4 | 70 | 8 | 60 | 1.9 | 265 | 0.1 |
| 90. | 3 Jul 79 | 10 | 10 | 290 | 7 | 330 | 11 | 1 | 6.0 | 247 | 4.2 |
| 89. | 1 May 79 | 30 | 16 | | | | | 12 | 1.5 | 99 | 1.6 |
| 88. | 22 Apr 79 | 220 | 13 | | | 190 | 13 | 201 | 8.3 | 76 | 1.3 |
| 87. | 17 Mar 79 | 280 | 9 | 300 | 2 | 315 | 3 | 235 | 6.1 | 267 | 3.1 |
| 86. | 4 Jan 79 | 250 | 6 | 270 | 6 | 270 | 9 | 225 | 3.9 | 230 | 4.3 |
| 85. | 26 Dec 78 | 240 | 10 | 210 | 5 | 200 | 7 | 249 | 6.5 | 265 | 4.4 |
| 84. | 27 Sep 78 | 60 | 10 | | | 60 | 9 | 58 | 6.6 | 42 | 7.4 |
| 83. | 18 Sep 78 | 260 | 6 | 120 | 2 | 170 | 6 | 191 | 3.5 | 83 | 1.6 |
| 82. | 22 Aug 78 | 30 | 8 | 0 | 4 | 65 | 14 | 35 | 7.9 | 17 | 5.6 |
| 81. | 4 Aug 78 | 210 | 7 | 260 | 7 | 165 | 6 | 207 | 5.7 | 199 | 4.4 |
| 80. | 17 Jul 78 | 30 | 9 | 330 | 2 | 0 | 4 | 311 | 3.5 | 210 | 2.8 |
| 79. | 8 Jul 78 | 200 | 6 | 200 | 10 | 180 | 11 | 186 | 3.9 | 56 | 2.8 |
| 78. | 29 Jun 78 | 0 | 11 | 300 | 8 | 20 | 9 | 340 | 7.2 | 242 | 0.7 |
| 77. | 20 Jun 78 | 280 | 5 | 60 | 5 | 105 | 7 | 207 | 5.6 | 181 | 6.1 |
| 76. | 11 Jun 78 | 140 | 8 | 250 | 2 | 195 | 11 | 151 | 4.3 | 174 | 4.3 |
| 75. | 9 Apr 78 | 30 | 10 | 10 | 6 | 350 | 6 | 34 | 8.5 | 26 | 1.6 |
| 74. | 31 Mar 78 | 160 | 8 | | | 300 | 4 | 200 | 4.0 | 310 | 1.9 |
| 73. | 4 Mar 78 | 340 | 18 | 320 | 13 | 325 | 14 | 342 | 13.7 | 12 | 6.2 |
| 72. | 27 Jan 78 | 260 | 22 | 250 | 17 | 250 | 20 | 251 | 19.6 | 209 | 8.0 |
| 71. | 28 Dec 77 | 30 | 11 | | | 0 | 7 | 25 | 4.4 | 260 | 3.0 |
| 70. | 22 Dec 77 | 270 | 13 | 290 | 5 | 290 | 12 | 273 | 10.2 | 342 | 3.9 |
| 69. | 11 Oct 77 | c | c | | | 195 | 6 | 260 | 0.8 | 62 | 2.7 |
| 68. | 29 Sep 77 | 0 | 13 | | | 330 | 10 | 233 | 9.5 | 245 | 3.2 |
| 67. | 11 Sep 77 | 0 | 13 | | | 330 | 10 | 354 | 9.9 | 38 | 4.8 |

| | Date | 1000 Hours EST Norfolk Dir. (°) | Norfolk Speed (knots) | Patuxent Dir. (°) | Patuxent Speed (knots) | Wachapreague Dir. (°) | Wachapreague Speed (knots) | 24-Hour Norfolk Dir. (°) | 24-Hour Norfolk Speed (knots) | 5-Day Norfolk Dir. (°) | 5-Day Norfolk Speed (knots) |
|---|---|---|---|---|---|---|---|---|---|---|---|
| 66. | 5 Sep 77 | 220 | 10 | 240 | 2 | 175 | 9 | 212 | 6.5 | 180 | 3.5 |
| 65. | 6 Aug 77 | 250 | 13 | | | 250 | 9 | 233 | 11.0 | 227 | 6.8 |
| 64. | 19 Jul 77 | 290 | 5 | 330 | 4 | 335 | 5 | 233 | 5.6 | 224 | 3.6 |
| 63. | 7 Jun 77 | 320 | 12 | | | 310 | 13 | 235 | 14.6 | 303 | 3.4 |
| 62. | 8 May 77 | 50 | 10 | 20 | 8 | 300 | 5 | 31 | 3.8 | 188 | 2.2 |
| 61. | 14 Apr 77 | 290 | 7 | 320 | 7 | 330 | 9 | 247 | 7.2 | 205 | 2.9 |
| 60. | 9 Mar 77 | 220 | 11 | 200 | 2 | 195 | 15 | 201 | 8.6 | 261 | 2.1 |
| 59. | 25 Feb 77 | 250 | 16 | 240 | 14 | 250 | 16 | 245 | 12.1 | 236 | 7.2 |
| 58. | 1 Feb 77 | 290 | 14 | 260 | 14 | 270 | 16 | 268 | 11.9 | 270 | 10.5 |
| 57. | 27 Dec 76 | 310 | 15 | 310 | 16 | 320 | 14 | 295 | 12.0 | 275 | 5.2 |
| 56. | 9 Dec 76 | 280 | 6 | 310 | 6 | 290 | 10 | 314 | 6.6 | 30 | 4.4 |
| 55. | 21 Nov 76 | 40 | 7 | 320 | 4 | 80 | 2 | 53 | 1.4 | 278 | 2.5 |
| 54. | 3 Nov 76 | 200 | 5 | | | 210 | 11 | 180 | 5.3 | 313 | 1.6 |
| 53. | 16 Oct 76 | 0 | 11 | 0 | 9 | 330 | 8 | 238 | 6.9 | 314 | 2.2 |
| 52. | 23 Aug 76 | 290 | 8 | 30 | 2 | 330 | 2 | 239 | 5.7 | 68 | 8.3 |
| 51. | 5 Aug 76 | 310 | 4 | | | 260 | 3 | 247 | 2.1 | 31 | 6.2 |
| 50. | 27 Jul 76 | 240 | 15 | | | | | | | | |
| 49. | 12 Jun 76 | 360 | 6 | | | | | 283 | 4.0 | 232 | 2.8 |
| 48. | 25 May 76 | 60 | 10 | | | | | | | | |
| 47. | 28 Apr 76 | 320 | 10 | 310 | 7 | 320 | 12 | 251 | 7.7 | 305 | 4.5 |
| 46. | 10 Apr 76 | 0 | 13 | 320 | 6 | 330 | 10 | 341 | 10.8 | 13 | 4.1 |
| 45. | 1 Apr 76 | 350 | 14 | 310 | 10 | 310 | 14 | 233 | 3.5 | 149 | 2.5 |
| 44. | 23 Mar 76 | 40 | 10 | 300 | 4 | 75 | 3 | 66 | 3.1 | 221 | 6.8 |
| 43. | 5 Mar 76 | 250 | 18 | 230 | 15 | 195 | 16 | 217 | 10.2 | 208 | 1.8 |
| 42. | 25 Feb 76 | 250 | 12 | 270 | 6 | 230 | 6 | 240 | 9.6 | 224 | 4.7 |
| 41. | 7 Feb 76 | 0 | 14 | 320 | 12 | 330 | 13 | 1 | 14.1 | 352 | 3.0 |
| 40. | 20 Jan 76 | 240 | 13 | 230 | 11 | 195 | 12 | 220 | 8.1 | 355 | 5.2 |
| 39. | 2 Jan 76 | 50 | 7 | 70 | 1 | 50 | 3 | 41 | 9.9 | 43 | 2.2 |
| 38. | 24 Dec 75 | 20 | 15 | 20 | 6 | 10 | 8 | 6 | 12.2 | 334 | 7.5 |
| 37. | 18 Nov 75 | 0 | 7 | 300 | 6 | 310 | 6 | 256 | 3.1 | 305 | 6.2 |
| 36. | 31 Oct 75 | 0 | 13 | 20 | 5 | 350 | 7 | 18 | 13.5 | 7 | 7.9 |
| 35. | 22 Oct 75 | 280 | 7 | 150 | 2 | 300 | 4 | 240 | 7.2 | 227 | 5.6 |
| 34. | 13 Oct 75 | 0 | 11 | 280 | 8 | 320 | 6 | 350 | 8.5 | 6 | 2.3 |
| 33. | 4 Oct 75 | 30 | 10 | 240 | 4 | 330 | 4 | 3 | 1.1 | 34 | 5.3 |

| | | 1000 Hours EST | | | | | | 24-Hour | | 5-Day | |
|---|---|---|---|---|---|---|---|---|---|---|---|
| | | Norfolk | | Patuxent | | Wachapreague | | Norfolk | | Norfolk | |
| | Date | Dir. (°) | Speed (knots) | Dir. (°) | Speed (knots) | Dir. (°) | Speed (knots) | Dir. (°) | Speed (knots) | Dir. (°) | Speed (knots) |
| 32. | 29 Aug 75 | 110 | 8 | 130 | 8 | 110 | 7 | 95 | 1.9 | 117 | 0.5 |
| 31. | 20 Aug 75 | 40 | 6 | 310 | 4 | 225 | c | 67 | 1.3 | 315 | 1.4 |
| 30. | 11 Aug 75 | 220 | 7 | | | | | 214 | 5.6 | 247 | 4.0 |
| 29. | 2 Aug 75 | 40 | 4 | 290 | 4 | 330 | 1 | 231 | 2.2 | 72 | 1.9 |
| 28. | 18 Jun 75 | 180 | 7 | 140 | 9 | 150 | 6 | 202 | 3.0 | 122 | 3.3 |
| 27. | 9 Jun 75 | 320 | 9 | 280 | 3 | 340 | 8 | 343 | 6.9 | 291 | 5.4 |
| 26. | 22 May 75 | 220 | 11 | | | | | 198 | 7.9 | 7 | 2.1 |
| 25. | 13 May 75 | 270 | 11 | | | | | 230 | 7.9 | 130 | 3.0 |
| 24. | 25 Apr 75 | 240 | 10 | | | 140 | 4 | 232 | 13.4 | 228 | 5.6 |
| 23. | 21 Feb 75 | 10 | 15 | 330 | 5 | 350 | 7 | 341 | 3.2 | 39 | 1.8 |
| 22. | 11 Dec 74 | c | c | | | 185 | 4 | 199 | 4.5 | 236 | 6.3 |
| 21. | 23 Nov 74 | 50 | 6 | | | 60 | 3 | 46G | 4.5 | 262G | 7.6 |
| 20. | 18 Oct 74 | 0 | 18 | c | c | 20 | 10 | 306 | 1.8 | 147 | 0.7 |
| 19. | 12 Sep 74 | 250 | 10 | 250 | 6 | 220 | 6 | 214 | 6.5 | 57 | 3.5 |
| 18. | 20 Jul 74 | 0 | 12 | 30 | 12 | 20 | 12 | 13 | 9.7 | 261 | 2.7 |
| 17. | 21 Apr 74 | 230 | 7 | 210 | 12 | 210 | 11 | 81 | 1.8 | 220 | 5.3 |
| 16. | 3 Apr 74 | 200 | 12 | 160 | 9 | 160 | 12 | 152 | 4.5 | 237 | 4.4 |
| 15. | 26 Feb 74 | 0 | 14 | 330 | 15 | 330 | 12 | 346 | 15.0 | 272 | 4.5 |
| 14. | 28 Nov 73 | 220 | 17 | | | | | | | | |
| 13. | 10 Nov 73 | 360 | 16 | | | | | 354 | 14.7 | 340 | 6.3 |
| 12. | 23 Oct 73 | 60 | 8 | 280 | 2 | 65 | 6 | 46 | 1.9 | 65 | 6.0 |
| 11. | 5 Oct 73 | 250 | 7 | | | | | 228 | 6.4 | 106 | 3.6 |
| 10. | 17 Sep 73 | 80 | 12 | | | | | | | | |
| 9. | 30 Aug 73 | 10 | 4 | | | 330 | 4 | 231 | 2.0 | 201 | 2.2 |
| 8. | 12 Aug 73 | 210 | 12 | 230 | 6 | 250 | 5 | 221 | 8.7 | 181 | 3.7 |
| 7. | 25 Jul 73 | 160 | 4 | | | | | | | | |
| 6. | 1 Jun 73 | 40 | 11 | 310 | 3 | 60 | 6 | 45 | 4.7 | 197 | 7.2 |
| 5. | 14 May 73 | 70 | 14 | | | | | | | | |
| 4. | 13 Feb 73 | 230 | 3 | c | c | 20 | 4 | 217 | 4.2 | 358 | 14.3 |
| 3. | 26 Jan 73 | 10 | 5 | 30 | 6 | 45 | 5 | 221 | 6.6 | 224 | 2.7 |
| 2. | 3 Dec 72 | 210 | 16 | 270 | 6 | 260 | 10 | 197 | 10.3 | 272 | 3.8 |
| 1. | 10 Oct 72 | 10 | 15 | 30 | 9 | 50 | 11 | 18 | 14.5 | 2 | 6.6 |

c - calm

G - Gloucester Point data.

TABLE 5

TIDE DATA FOR LANDSAT PASSES

Overpass Time Before (-) or After (+)

Actual High Tide at Sewells Point

| | Date | Time Difference |
|---|---|---|
| 94. | 3 Dec 79 | + 1:06 |
| 93. | 15 Nov 79 | + 4:18 |
| 92. | 28 Oct 79 | - 5:00 |
| 91. | 19 Oct 79 | + 3:10 |
| 90. | 3 Jul 79 | - 4:35 |
| 89. | 1 May 79 | - 1:09 |
| 88. | 22 Apr 79 | + 4:41 |
| 87. | 17 Mar 79 | - 1:26 |
| 86. | 4 Jan 79 | - 2:44 |
| 85. | 26 Dec 78 | + 4:33 |
| 84. | 27 Sep 78 | + 5:45 |
| 83. | 18 Sep 78 | + 0:50 |
| 82. | 22 Aug 78 | - 0:57 |
| 81. | 4 Aug 78 | + 1:51 |
| 80. | 17 Jul 78 | + 5:08 |
| 79. | 8 Jul 78 | - 0:14 |
| 78. | 29 Jun 78 | - 5:34 |
| 77. | 20 Jun 78 | + 2:28 |
| 76. | 11 Jun 78 | - 1:47 |
| 75. | 9 Apr 78 | - 0:18 |
| 74. | 31 Mar 78 | - 3:23 |
| 73. | 4 Mar 78 | + 5:11 |
| 72. | 27 Jan 78 | - 1:52 |
| 71. | 28 Dec 77 | - 2:07 |
| 70. | 22 Dec 77 | + 2:44 |
| 69. | 11 Oct 77 | + 3:05 |
| 68. | 29 Sep 77 | - 0:09 |
| 67. | 11 Sep 77 | + 2:17 |
| 66. | 5 Sep 77 | - 3:41 |
| 65. | 6 Aug 77 | - 4:27 |
| 64. | 19 Jul 77 | - 1:01 |
| 63. | 7 Jun 77 | - 2:54 |
| 62. | 8 May 88 | - 2:36 |
| 61. | 14 Apr 77 | + 4:39 |
| 60. | 9 Mar 77 | - 1:56 |
| 59. | 25 Feb 77 | - 3:47 |
| 58. | 1 Feb 77 | + 2:24 |
| 57. | 27 Dec 76 | - 4:11 |
| 56. | 9 Dec 76 | - 0:58 |
| 55. | 21 Nov 76 | + 1:20 |
| 54. | 3 Nov 76 | + 3:22 |
| 53. | 16 Oct 76 | - 3:32 |
| 52. | 23 Aug 76 | + 3:48 |
| 51. | 5 Aug 76 | - 6:30 |
| 50. | 27 Jul 76 | + 1:25 |
| 49. | 12 Jun 76 | + 2:02 |
| 48. | 25 May 76 | + 4:50 |
| 47. | 28 Apr 76 | + 2:02 |
| 46. | 10 Apr 76 | + 4:15 |
| 45. | 1 Apr 76 | + 0:09 |
| 44. | 23 Mar 76 | - 5:56 |
| 43. | 5 Mar 76 | - 2:01 |
| 42. | 25 Feb 76 | + 4:17 |
| 41. | 7 Feb 76 | - 3:25 |
| 40. | 20 Jan 76 | - 1:25 |
| 39. | 2 Jan 76 | + 0:23 |
| 38. | 24 Dec 75 | - 3:20 |
| 37. | 18 Nov 75 | + 1:30 |
| 36. | 31 Oct 75 | + 3:49 |
| 35. | 22 Oct 75 | + 1:06 |
| 34. | 13 Oct 75 | - 5:21 |
| 33. | 4 Oct 75 | + 3:00 |
| 32. | 29 Aug 75 | - 2:41 |
| 31. | 20 Aug 75 | + 2:53 |
| 30. | 11 Aug 75 | - 1:05 |
| 29. | 2 Aug 75 | - 5:42 |
| 28. | 18 Jun 75 | - 6:04 |
| 27. | 9 Jun 75 | + 2:34 |
| 26. | 22 May 75 | + 4:17 |
| 25. | 13 May 75 | + 0:44 |
| 24. | 25 Apr 75 | + 2:20 |
| 23. | 21 Feb 75 | + 5:15 |
| 22. | 11 Dec 74 | + 2:48 |
| 21. | 23 Nov 74 | + 5:31 |
| 20. | 18 Oct 74 | - 0:04 |
| 19. | 12 Sep 74 | + 6:09 |
| 18. | 20 Jul 74 | + 1:17 |
| 17. | 21 Apr 74 | + 2:02 |

| | Date | Time Difference |
|---|---|---|
| 16. | 3 Apr 74 | + 4:38 |
| 15. | 26 Feb 74 | - 1:15 |
| 14. | 28 Nov 73 | - 1:01 |
| 13. | 10 Nov 73 | + 1:47 |
| 12. | 23 Oct 73 | + 4:30 |
| 11. | 5 Oct 73 | - 5:06 |
| 10. | 17 Sep 73 | - 0:29 |
| 9. | 30 Aug 73 | + 0:49 |
| 8. | 12 Aug 73 | + 3:19 |
| 7. | 25 Jul 73 | - 5:47 |
| 6. | 1 Jun 73 | + 2:21 |
| 5. | 14 May 73 | + 4:14 |
| 4. | 13 Feb 73 | + 5:08 |
| 3. | 26 Jan 73 | - 4:16 |
| 2. | 3 Dec 72 | + 2:32 |
| 1. | 10 Oct 72 | + 0:44 |

## 7. REFERENCES


Bumpus, D.F. 1973. A description of the circulation on the continental shelf of the east coast of the United States. In Progress in Oceanography (Ed. B.F. Warren), 6:111-156. Pergamon Press, N.Y.

Caponi, E.A. 1974. A three-dimensional model for the numerical simulation of estuaries. Ph.D. Thesis, Institute for Fluid Dynamics and Applied Mathematics, Univ. of Maryland, College Park, MD, 215 p.

Carron, M. 1979. The Virginia Chesapeake Bay: Recent sedimentation and paleodrainage. Ph.D. Dissertation, College of William and Mary, Williamsburg, VA, 83 p. + app.

Chen, H.S. 1978. A storm surge model study, volume II, A finite element storm surge analysis and its application to a bay - ocean system. VIMS Spec. Rept. No. 189, Gloucester Point, VA, 149 p.

Doebler, H.J. 1966. A study of shallow water drift currents at two stations off the east coast of the United States. U.S. Navy Underwater Sound Laboratory, Rept. 755, New London, Conn., 78 p.

Elder, R.B. 1971. The effect of run-off from Hurricane Camille on the continental shelf waters of the Chesapeake Bight. M.S. Thesis, College of William and Mary, Williamsburg, VA, 80 p.

Harrison, W., J.J. Norcross, N.A. Pore, and E.M. Stanley. 1967. Circulation of shelf waters off the Chesapeake Bight. ESSA Prof. Paper No. 3, U.S. Dept. Commerce, Washington, D.C., 82 p.

Howe, M.R. 1952. Some direct measurements of the non tidal drift on the continental shelf between Cape Cod and Cape Hatteras. Deep Sea Research 9:445-455.

Johnson, R.E. 1976. Circulation study near Cape Henry, Virginia, using Lagrangian techniques. Techn. Rep. No. 21, Inst. Oceanography, Old Dominion Univ., Norfolk, VA, 80 p. + app.

Ludwick, J.C. and J.R. Melchor. 1972. Surface water turbidity in the entrance to Chesapeake Bay, Virginia. Old Dominion Univ. Inst. of Oceanography Techn. Rep. 5, 67 p.

Ludwick, J.C. 1973. Tidal currents, sediment transports, and sand banks in Chesapeake Bay entrance, Virginia. Old Dominion Univ. Inst. of Oceanography Techn. Rep. 16, 13 p.

Mairs, R.L. and D.K. Clark. 1973. Remote sensing of estuarine circulation dynamics. Photogramm. Eng. 39(9):927-938.

Munday, J.C., Jr. and M.S. Fedosh. 1980. Southern Chesapeake Bay circulation and suspended sediment transport analyzed using Landsat imagery. Proc. Amer. Soc. Photogr. Fall Techn. Mtg., Niagara Falls, N.Y., p. RS-3-F:1-5.

Munday, J.C., Jr. and M.S. Fedosh. 1981. Chesapeake Bay plume dynamics from Landsat. Proc. Superflux Symp. on Results of the 1980 Chesapeake Bay Plume Study, Sponsored by Northeast Fisheries Center, NMFS, NOAA, Jan. 21-23, Williamsburg, VA, 15 p., in press.

Ruzecki, E.P., C. Welch, J. Usry, and J. Wallace. 1976. The use of the EOLE satellite system to observe continental shelf circulation. Eighth Ann. Offshore Techn. Conf., Houston, TX, p. 697-708.

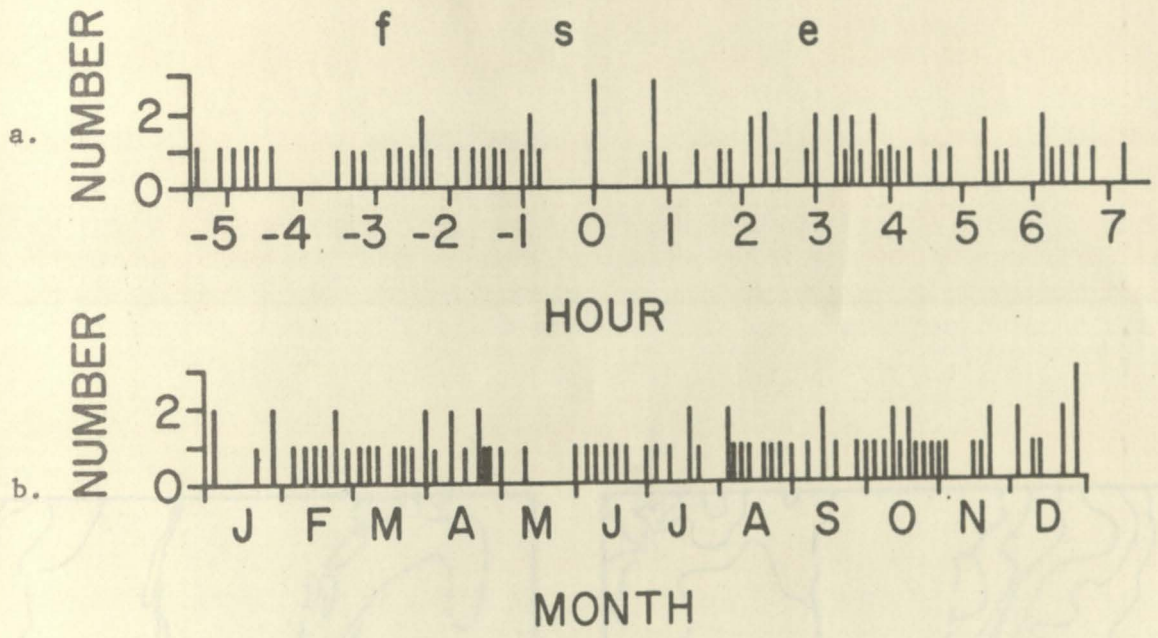


Figure 1. Tidal phases (1a:top) and seasonal distribution (1b:bottom) for Landsat overpasses of southern Chesapeake Bay. Tidal reference: high tide at Sewells Point, Hampton Roads.

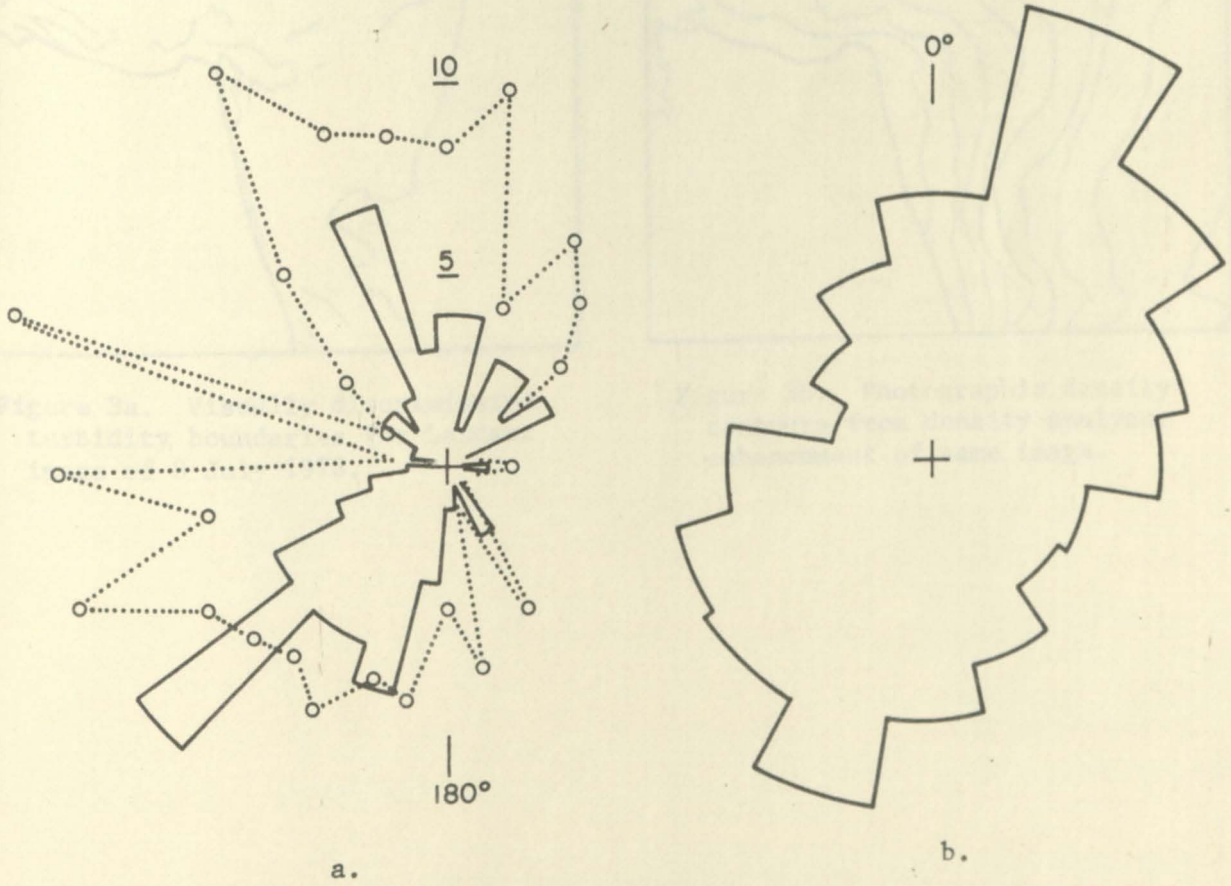


Figure 2. Winds at Norfolk Regional Airport.
a. Landsat passes. Solid line: wind frequency. Dotted line: average wind speed in knots.
b. The record for 1946-1970. Wind frequency only.

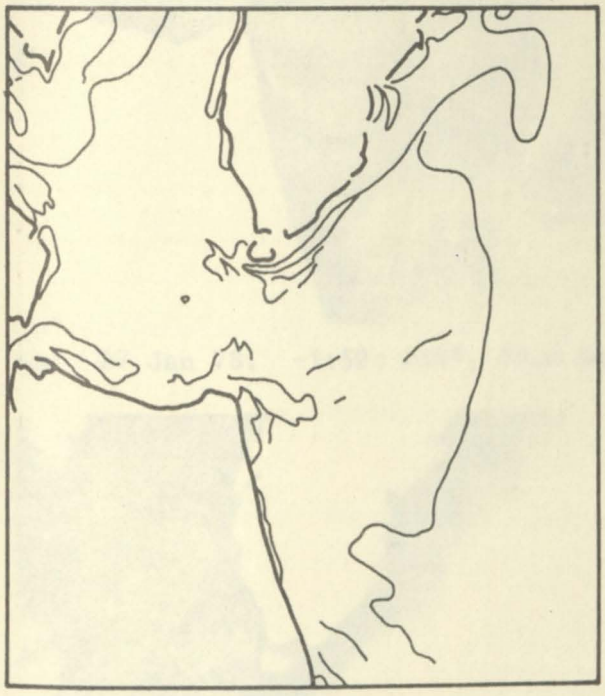

Figure 3a. Visually discriminated turbidity boundaries for Landsat image of 8 July 1978.

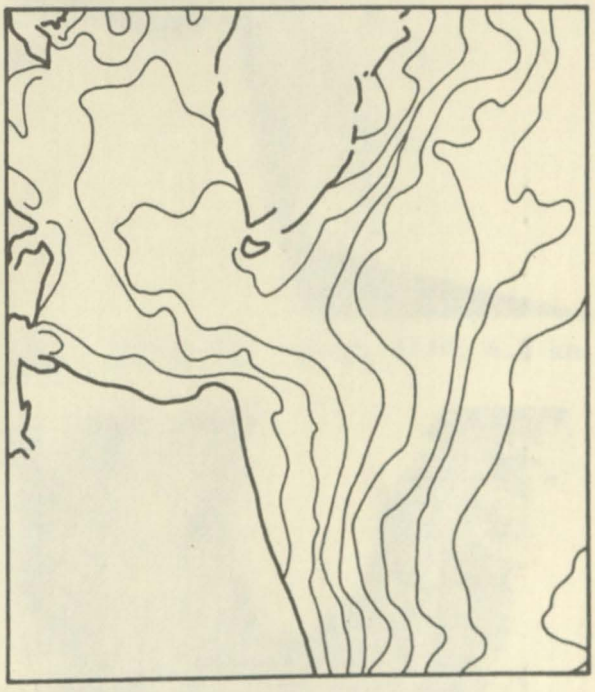

Figure 3b. Photographic density contours from density analyzer enhancement of same image.

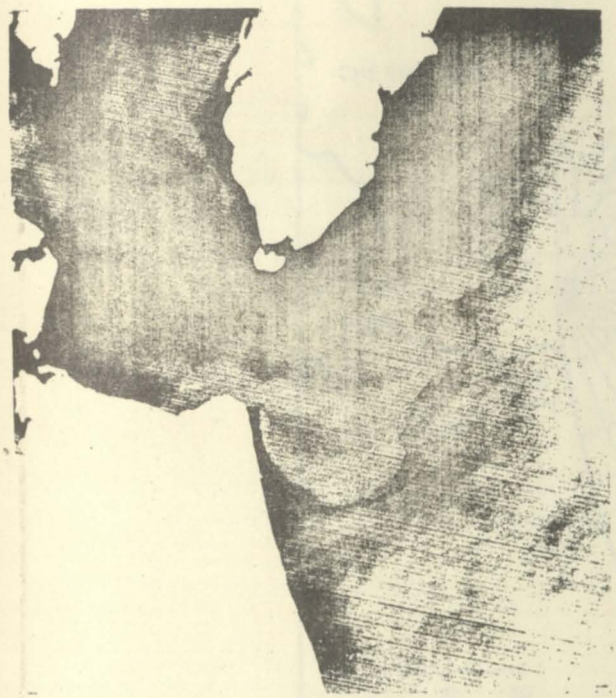

4a. 27 Jan 78. -1:52; 251°, 19.6 kn.

4b. 13 Feb 73. +5:08; 217°, 4.2 kn.

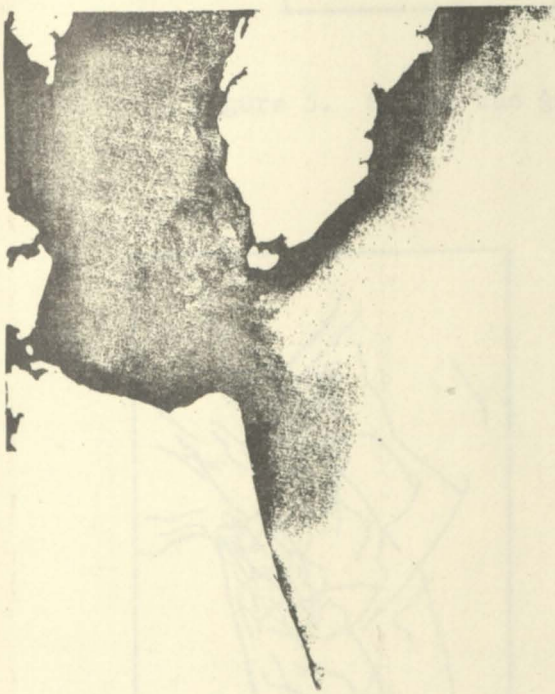

4c. 19 Oct 79. +3:07; 60°, 1.9 kn.

4d. 11 Sep 77. +2:17; 354°, 9.9 kn.

Figure 4. Landsat images of the Chesapeake Bay plume. MSS 5 negatives with masking of land areas. Top is north. Tides: hours before (-) or after (+) high tide at Cape Henry. Winds: 12 hour average from Norfolk. Scale 1:$10^6$.

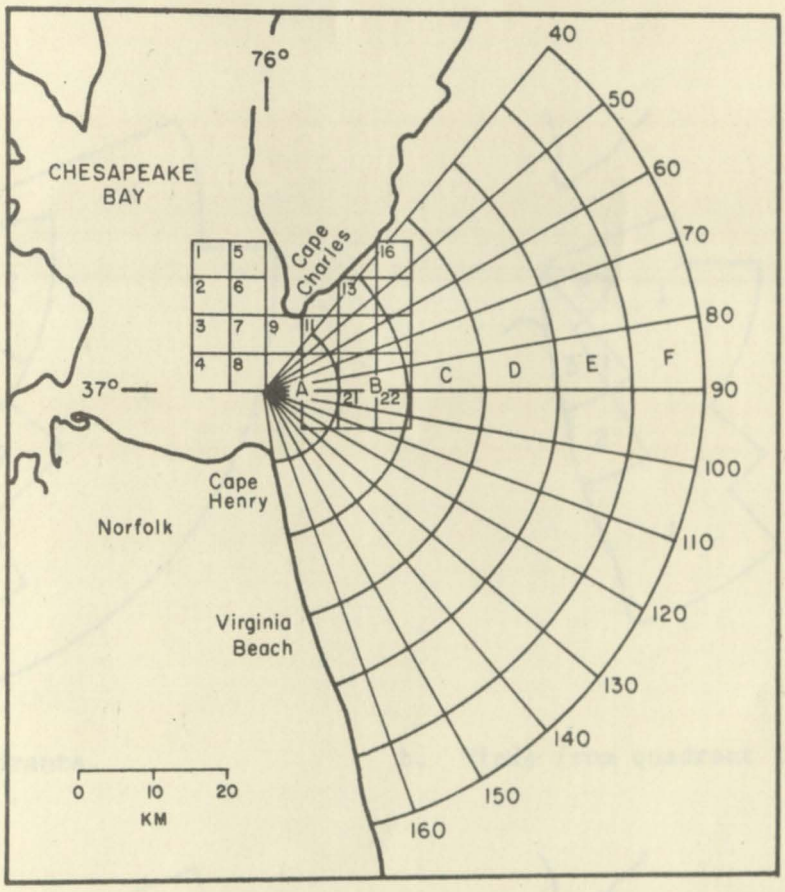


Figure 5. Sector and grid map for image data extraction.

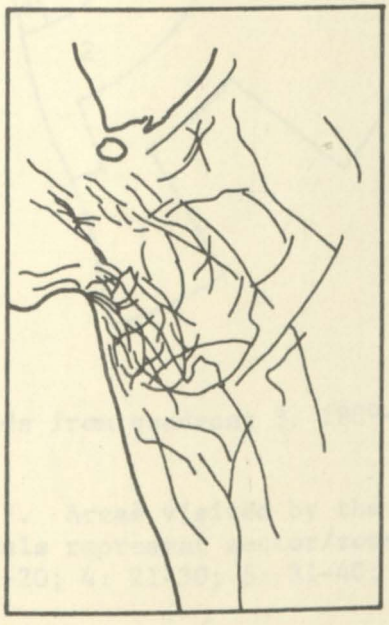

Figure 6a. Composite of turbidity boundaries for flood tide.

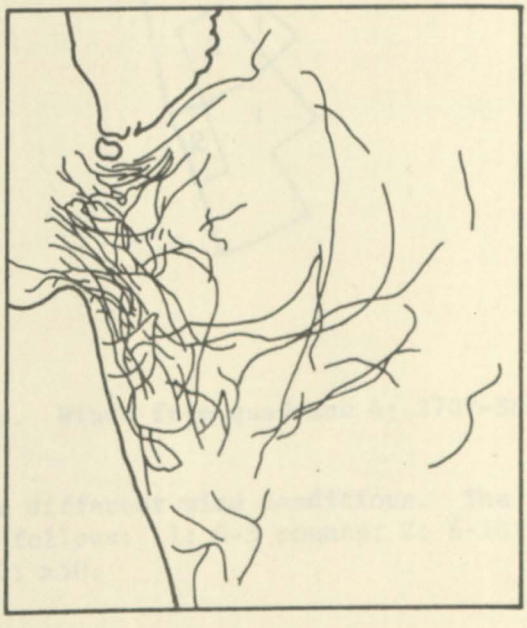

Figure 6b. Composite of turbidity boundaries for ebb tide.

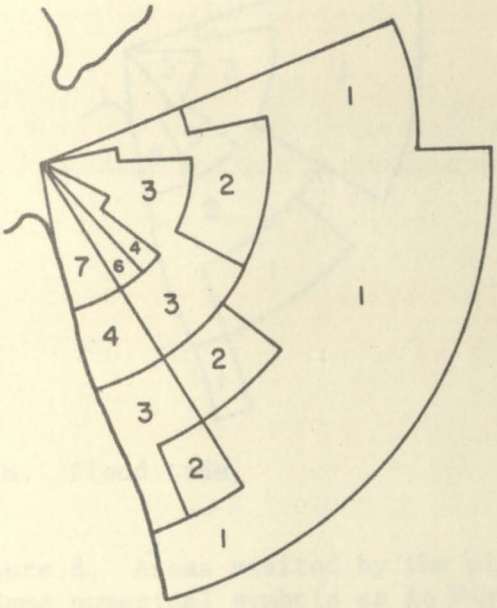


a. All wind quadrants.

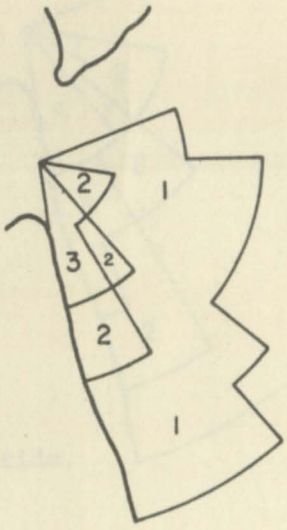


b. Winds from quadrant 1: 0°-90°.

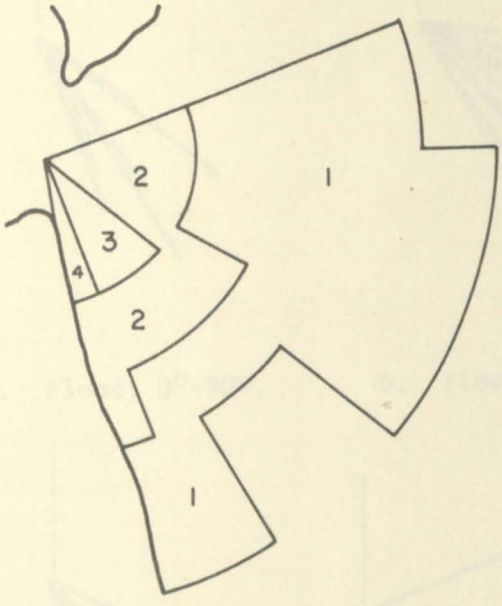


c. Winds from quadrant 3: 180°-270°.

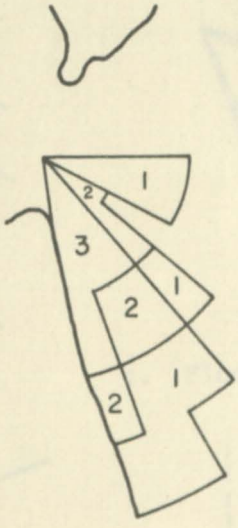


d. Winds from quadrant 4: 270°-360°.

Figure 7. Areas visited by the plume under different wind conditions. The numerals represent sector/zone counts as follows: 1: 0-5 counts; 2: 6-10; 3: 11-20; 4: 21-30; 5: 31-40; 6: 41-50; 7: >50.

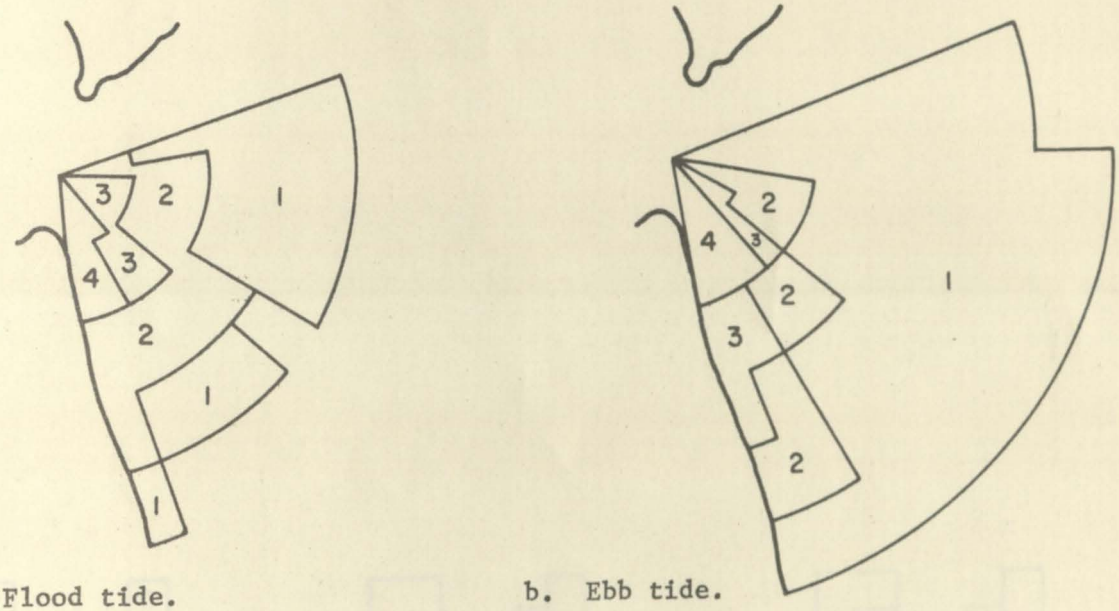


a. Flood tide. b. Ebb tide.

Figure 8. Areas visited by the plume under different tidal phases. Same numerical symbols as in Figure 7.

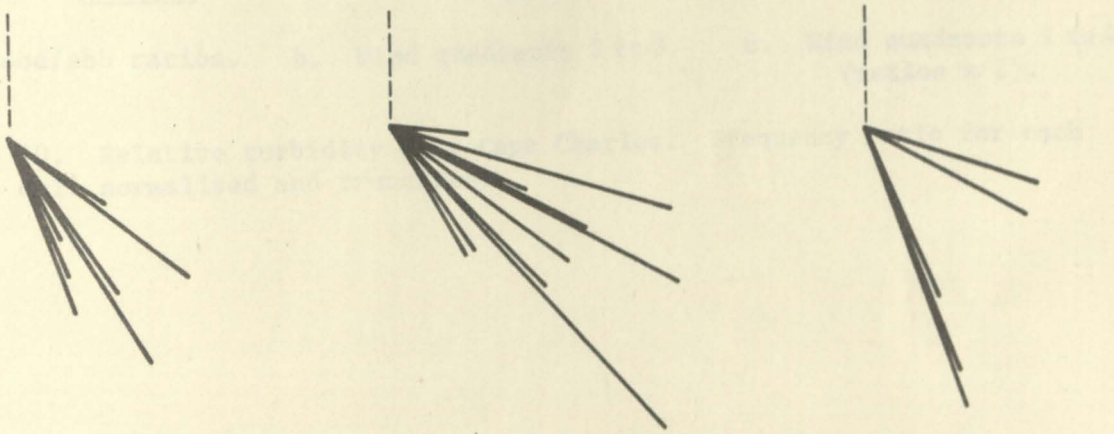

a. Flood; 0°-90°. b. Flood; 180°-270°. c. Flood; 270°-360°.

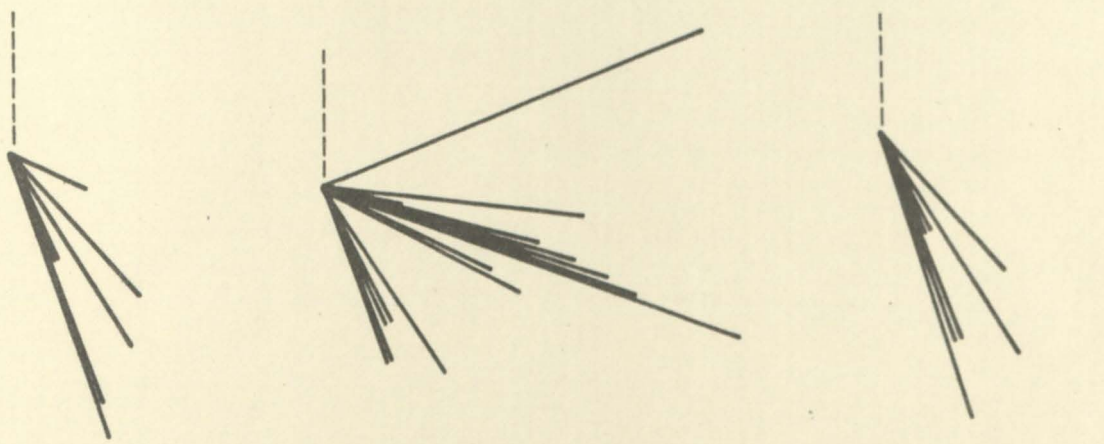

d. Ebb; 0°-90°. e. Ebb; 180°-270°. f. Ebb; 270°-360°.

Figure 9. Plume extension under different tidal and wind conditions. Radial lines for the most distant point on each plume. North shown as dotted line.

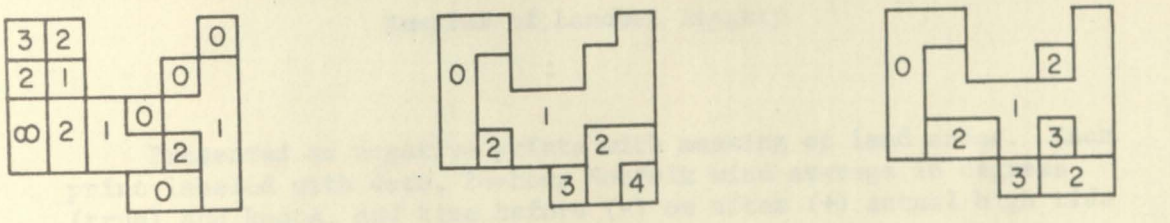


a. Flood/ebb ratios. b. Wind quadrants 1 to 3. c. Wind quadrants 1 to 4 (ratios x 2).

Figure 10. Relative turbidity near Cape Charles. Frequency ratio for each grid cell normalized and truncated.

# APPENDIX

## Samples of Landsat Imagery

Presented as negative prints with masking of land areas. Each print labeled with date, 24-hour Norfolk wind average in degrees (true) and knots, and time before (-) or after (+) actual high tide at Sewells Point, Hampton Roads.

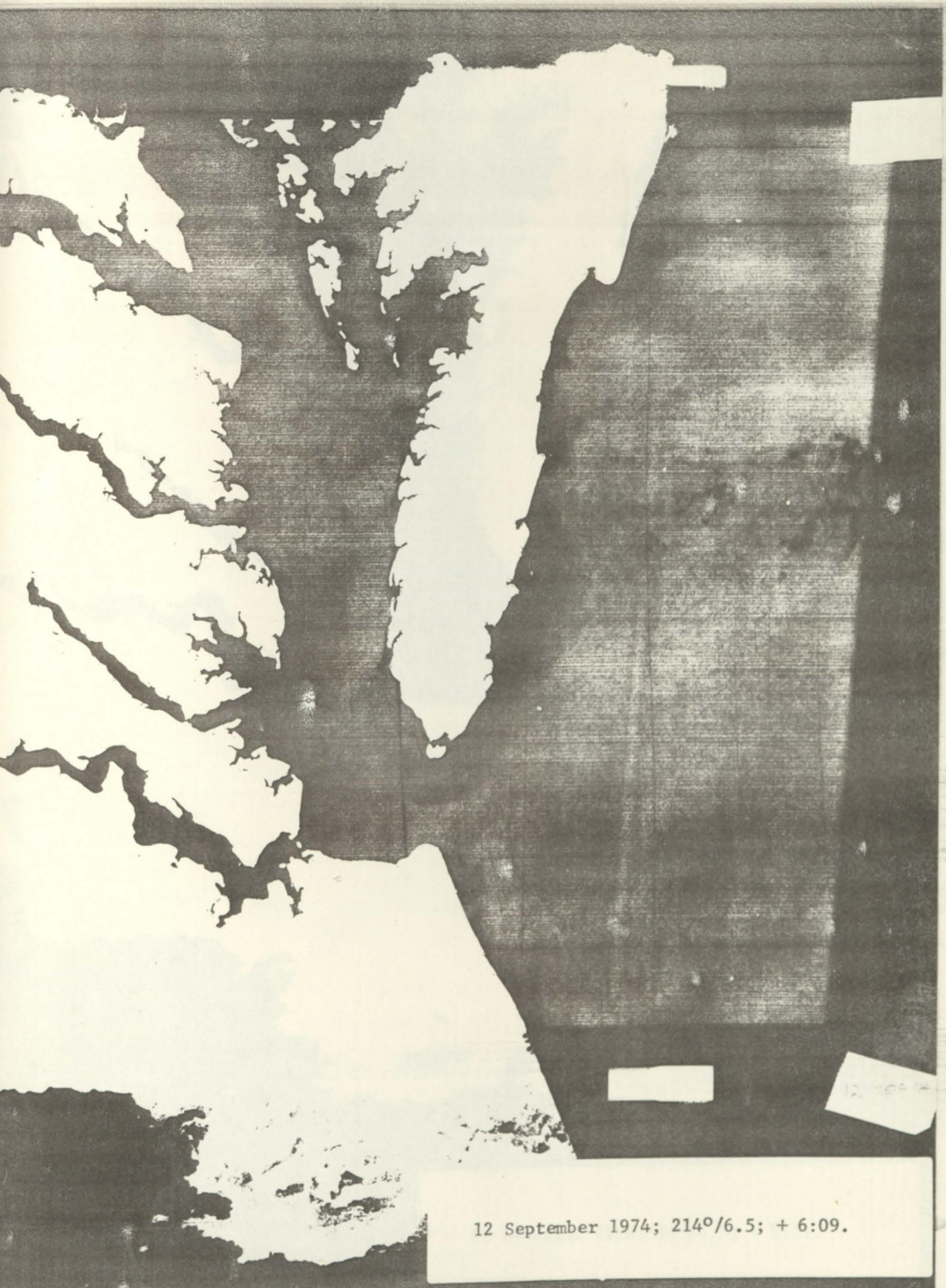

12 September 1974; 214°/6.5; + 6:09.

23 November 1974; 46°/4.5; + 5:31.

21 February 1975; 341°/3.2; + 5:15.

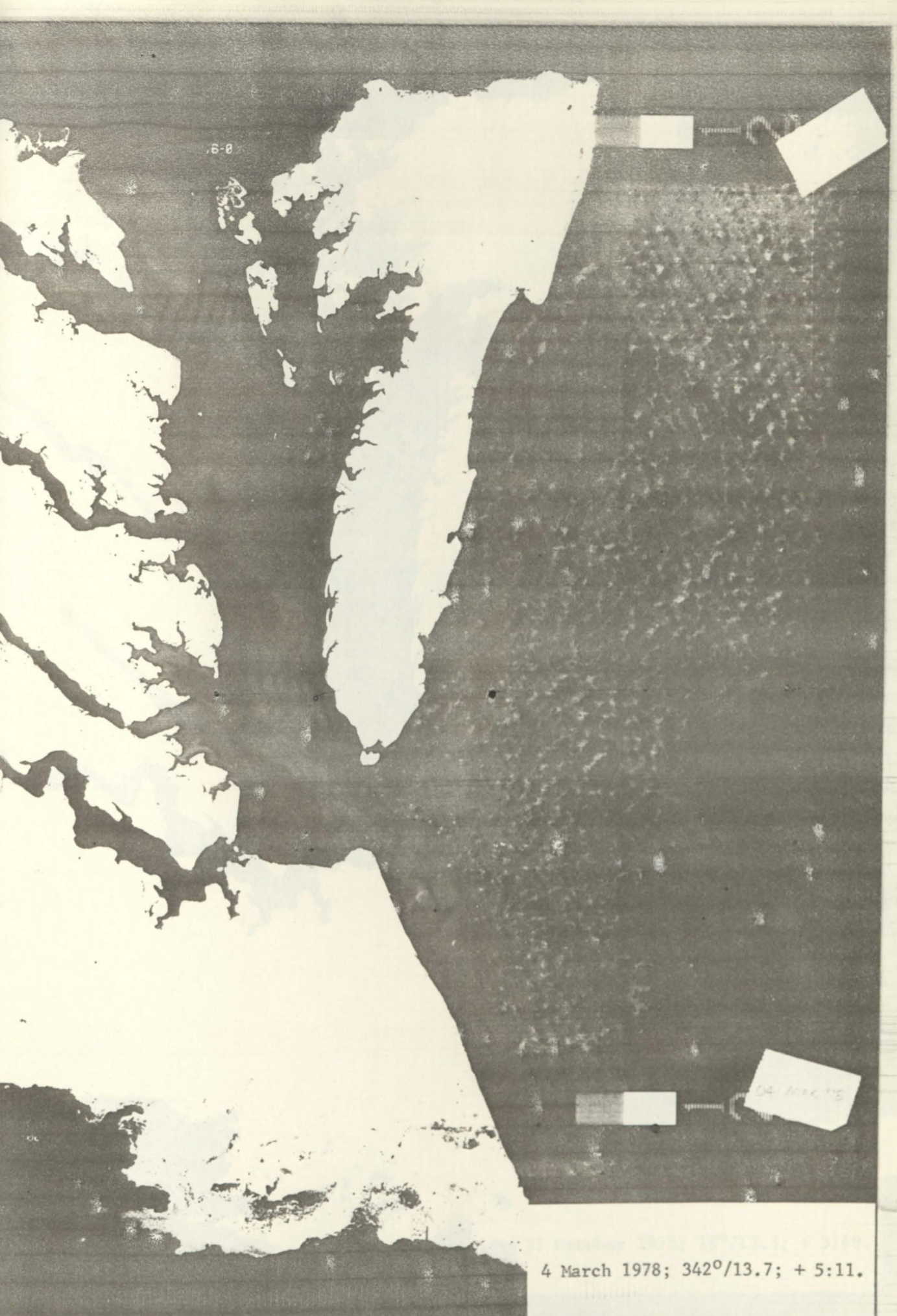

4 March 1978; 342°/13.7; + 5:11.

31 October 1975; 18°/13.5; + 3:49.

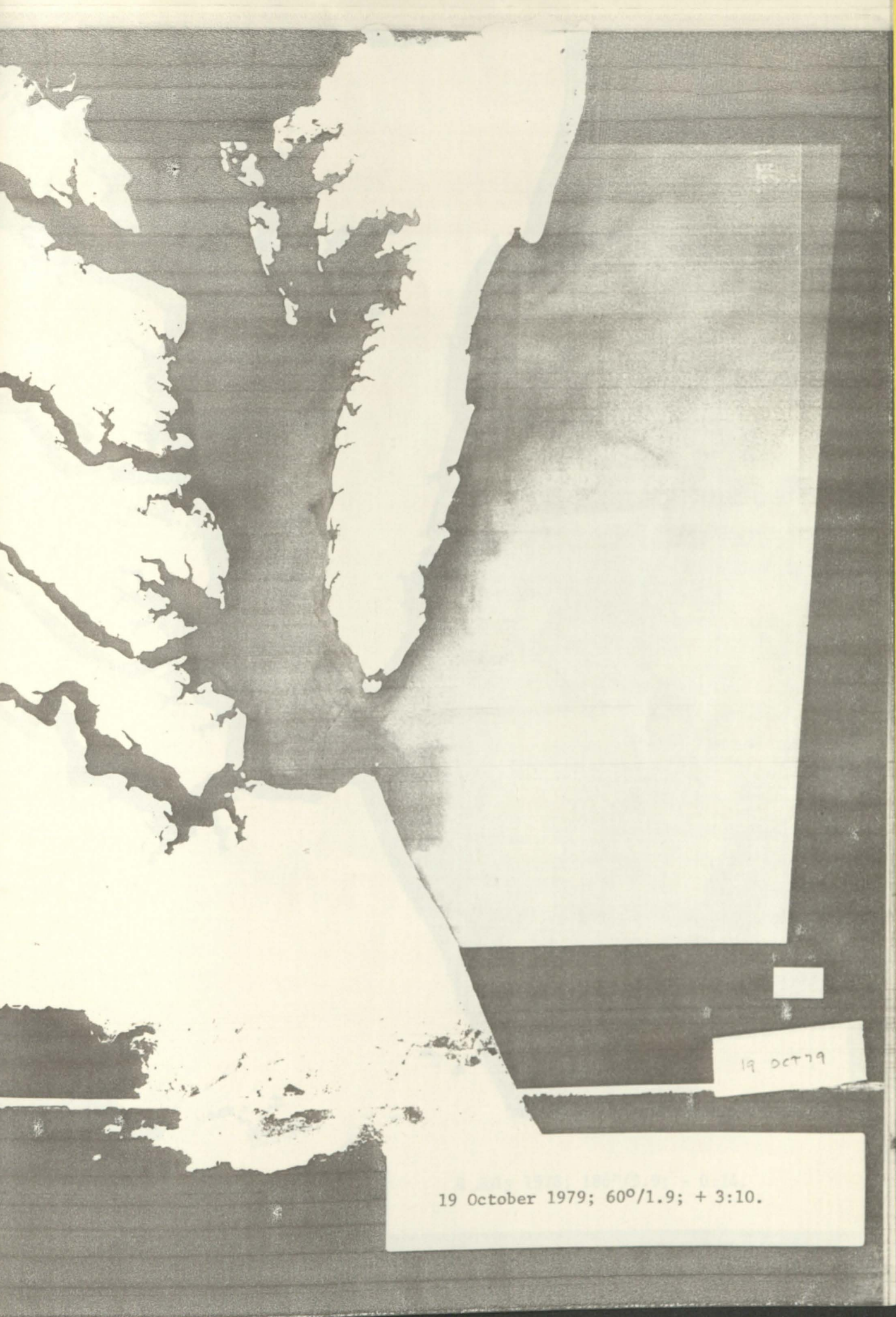


19 October 1979; 60°/1.9; + 3:10.

8 July 1978; 186°/3.9; - 0:14.

09 DEC

9 December 1976; 314°/6.6; - 0:58.

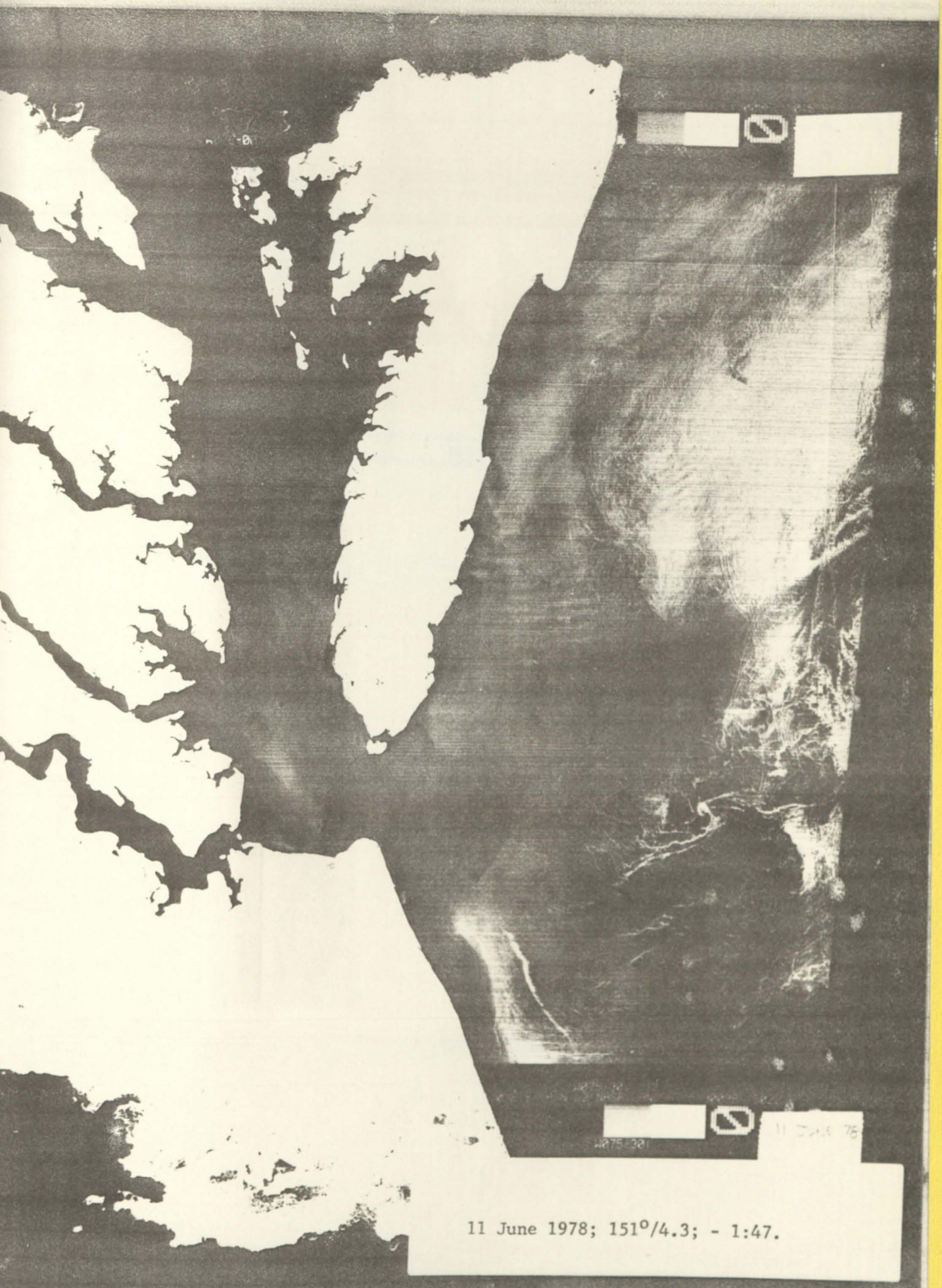

11 June 1978; 151°/4.3; - 1:47.